Characterization of Hydrogen Bonding Motifs in Proteins:

Hydrogen Elimination Monitoring by Ultraviolet Photodissociation Mass Spectrometry

Lindsay J. Morrison, Wenrui Chai, Jake A. Rosenberg, Graeme Henkelman, and Jennifer S Brodbelt*

Department of Chemistry, University of Texas, Austin, TX 78712

Correspondence to: jbrodbelt@cm.utexas.edu

Supporting Information

Error Analysis:

The errors associated with assignment of α_a values from experimental data fundamentally depend on the accuracy with which the ^{13}C isotopes of the overlapping *a*/*a*+1 ions can be correctly deconvolved. We observed an apparent reduction in the accuracy for ions larger than approximately 7000 Da due to a decrease in the changes in RMSD of the error between an experimental isotope distribution and a theoretical fit as a function of assigned α_a values. This concept is illustrated in **Figure S1**, wherein a plot of the RMSD of fits to the a_{66}^{4+} fragment is shown as a function of α_a value. Solving the fit using RMSD as a criterion results in optimization of α_a to 0.32 with an RMSD of 0.15. However, α_a value fits of 0.20 and 0.40 provide only subtly less optimal fits with RMSDs of 0.17 and 0.16, respectively. Hence, ions having weak or irregular isotope distributions due to low abundance or low S/N are prone to errors in assignment of α_a values; owing to the similarity of RMSD for fits of larger ions, this problem is exacerbated with increasing fragment mass. To assess the limits of the accuracy of the isotope deconvolution procedure, $\Delta_{\alpha a=0.1}$RMSD was defined as the difference in RMSD of the fit at an α_a value that differ by 0.1 from the optimized value and was calculated for a series of fragments with relatively good signal abundances from Scp1. Previous study of α_a values for LysN peptides demonstrated that backbone cleavage at a particular amino acid was reproducible with standard deviations of approximately 0.1, which reflects normal variations in the peptide behavior. Thus, $\Delta_{\alpha a=0.1}$RMSD defines the change in RMSD that would be expected for a fit within ±0.1 of the correct, optimized α_a value. Theoretically, the curve that defines ΔRMSD as a function of α_a follows an absolute value function with curvature arising from natural error of the fit; this is shown in for the a_{66}^{4+} fragment of Scp1 in **Figure S2a**. Hence, $\Delta_{\alpha a=0.1}$RMSD is a convenient measure of the slope of the absolute value function for real data. In **Figure S2b** and **c**, $\Delta_{\alpha a=0.1}$RMSD is shown as a function of mass for idealized fits and actual fits for several fragments from Scp1. The results from both the theoretical (perfect) fits and experimental fits were found to fit well to power functions and trend lines are shown accordingly on the on the plots in **Figure S2**. For comparison, the theoretical and experimental RMSD of a smaller ion, the a_{37}^{3+} (mass ≈ 4000 Da) from Scp1, is shown in **Figure S2d**. Inspection of the increased slopes of these curves relative to those in **Figure S1** and **S2a** demonstrates the effect of mass on the optimization function. The plots in Figure **S2b** and **2c** feature a reduction in $\Delta_{\alpha a=0.1}$RMSD with increasing mass, consistent with a decrease in the slope of the absolute value function of ΔRMSD versus α_a and together suggesting a limit for which accurate fitting can be achieved. Given that the $\Delta_{\alpha a=0.1}$RMSD of the largest ion studied, having a mass of 7340 Da, was 0.02, we empirically take this value as the lower limit for obtaining an accurate fit of an experimental isotope distribution. Using the regression from the experimental fits, 7440 Da was found to be the theoretical limit for determination of α_a within ±0.1. This value is somewhat empirical and depends on the abundance and S/N for a given ion, and theoretically an ion having a mass larger than 7440 Da could be accurately fit if the RMSD was relatively low. However, $\Delta_{\alpha a=0.1}$RMSD provides a reasonable indication of the optimization. For the present study, all fragment ions having a $\Delta_{\alpha a=0.1}$RMSD of less than 0.02 were discarded from the analysis.

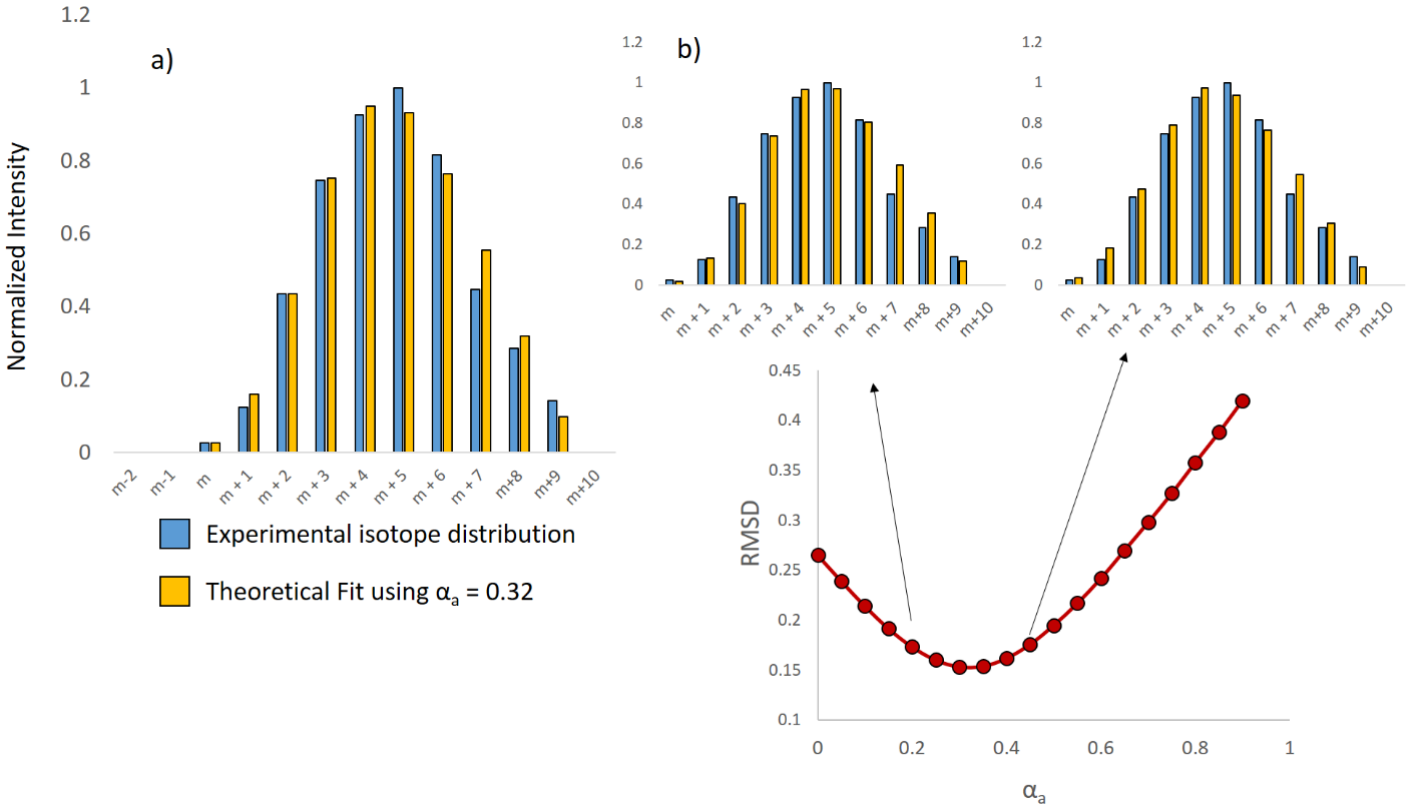

Figure S1: The experimental isotope distribution and theoretical fit using $\alpha_a = 0.32$ for the a_{66}^{4+} fragment of Scp1 (9+) is shown in a) and the RMSD of the fits for α_a between 0.0 and 0.9 is shown in b). Insets show the fits at $\alpha_a = 0.2$ and 0.4, demonstrating the subtle differences in fits as a function of α_a for ions larger than 7000 Da.

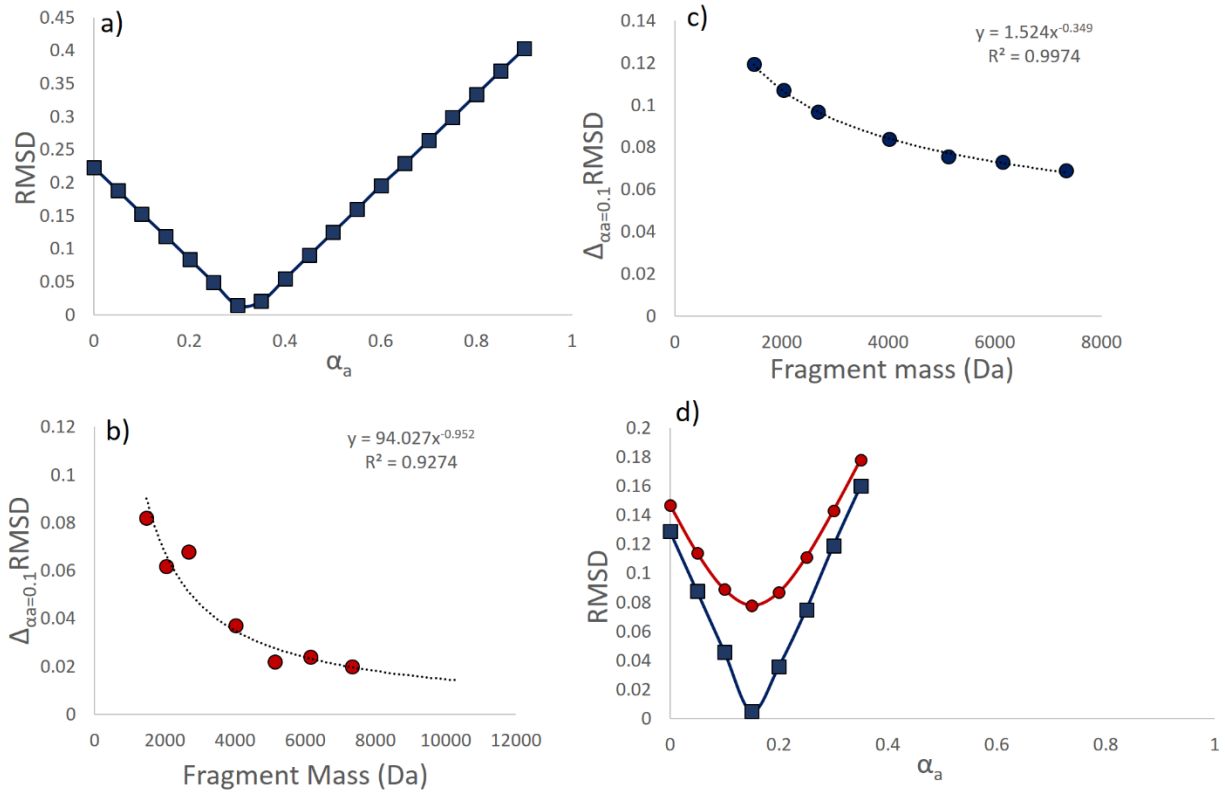

Figure S2: The theoretical RMSD as a function of α_a is plotted for the a_{66}^{4+} fragment of Scp1 in a). In b) and c), $\Delta_{\alpha a=0.1}$RMSD is plotted as a function of fragment mass for theoretical and experimental fits, respectively, of several fragment ions from Scp1. In d), RMSD is plotted as a function of α_a for the smaller a_{37}^{3+} ion (≈4000 Da) of Scp1 to demonstrate the effect that fragment ion mass has on the α_a optimization function. The red curve is the experimental RMSD; the blue curve is the theoretical RMSD.

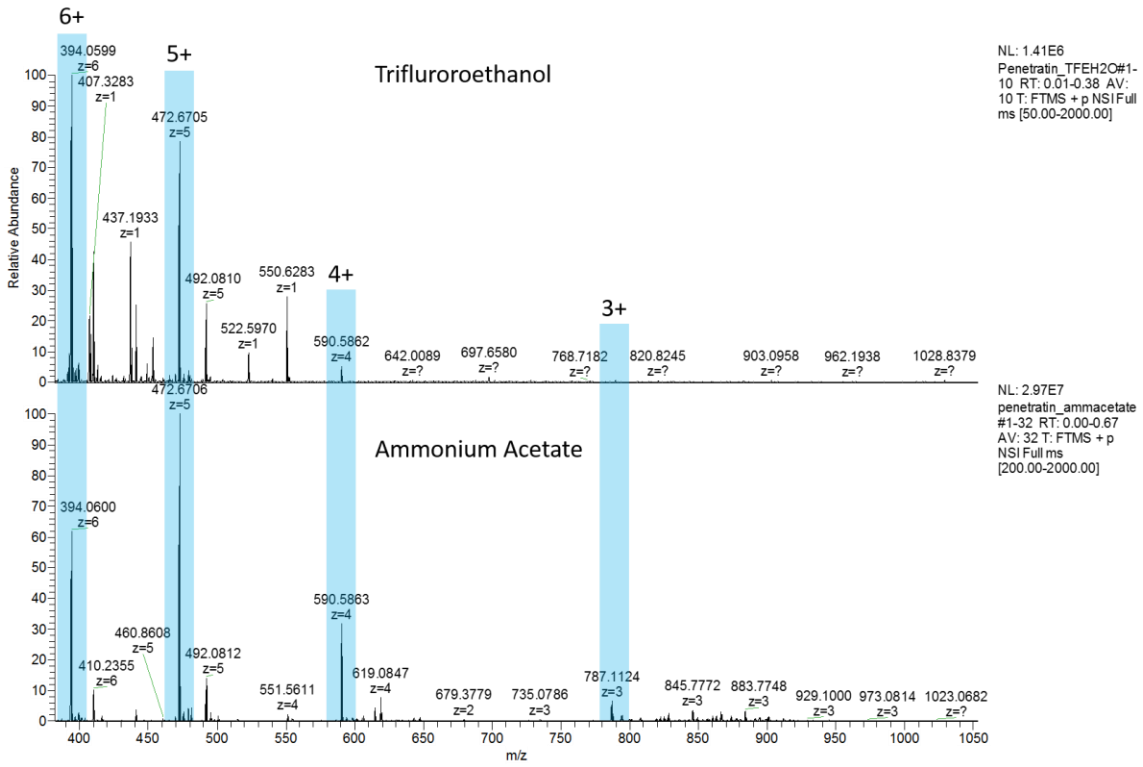

Figure S3: MS1 spectra of penetratin-Arg sprayed from a) 50:50 H_2O/trifluoroethanol and b) 50 mM ammonium acetate.

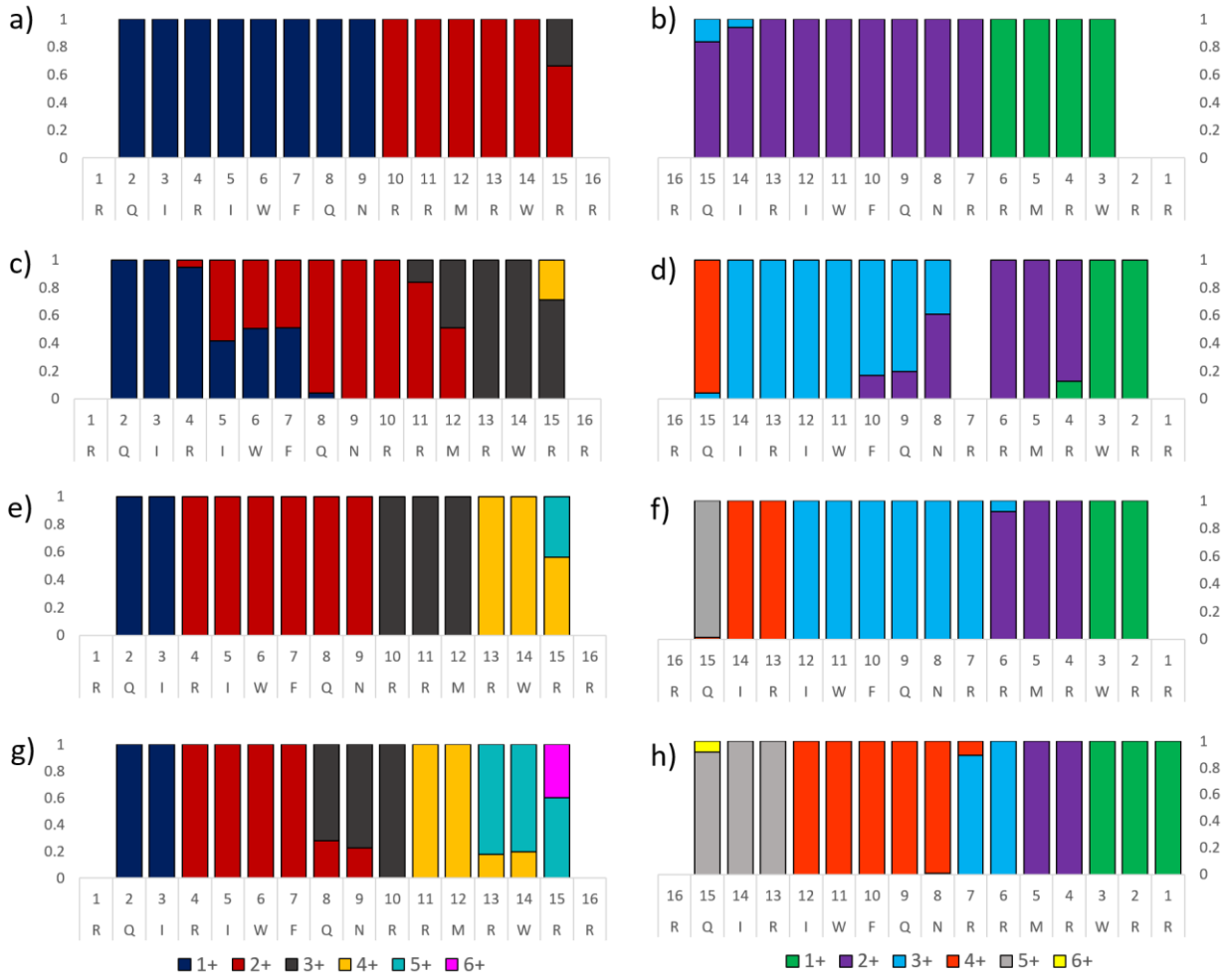

Figure S4: Charge site analysis of the 3+ (a and b), 4+ (c and d), 5+ (e and f), and 6+ (g and h) charge states of penetratin-Arg. The *a* ion series is shown in a, c, e, and g, and the *x* ion series is shown in b, d, f, and h.

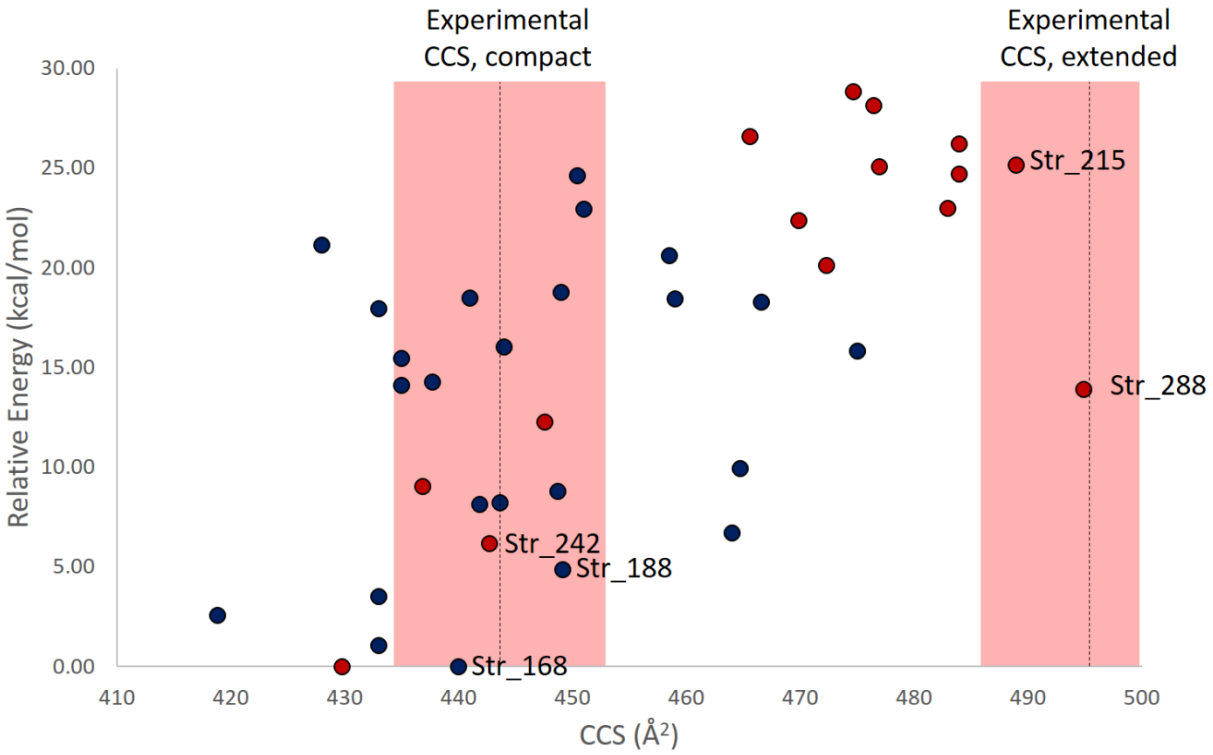

Figure S5: Predicted collisional cross sections and relative energies of the 40 lowest energy structures of penetratin-Arg (5+) obtained from MD modeling. Structures generated using the NMR structure as the starting conformation are shown in blue, and structures generated using a fully helical starting conformation are shown in red. Black dashed lines denote the experimental CCS of the compact and elongated populations of penetratin-Arg (5+) based on ion mobility measurements. The pink shaded regions denote ±2% CCS from the compact and extended populations.

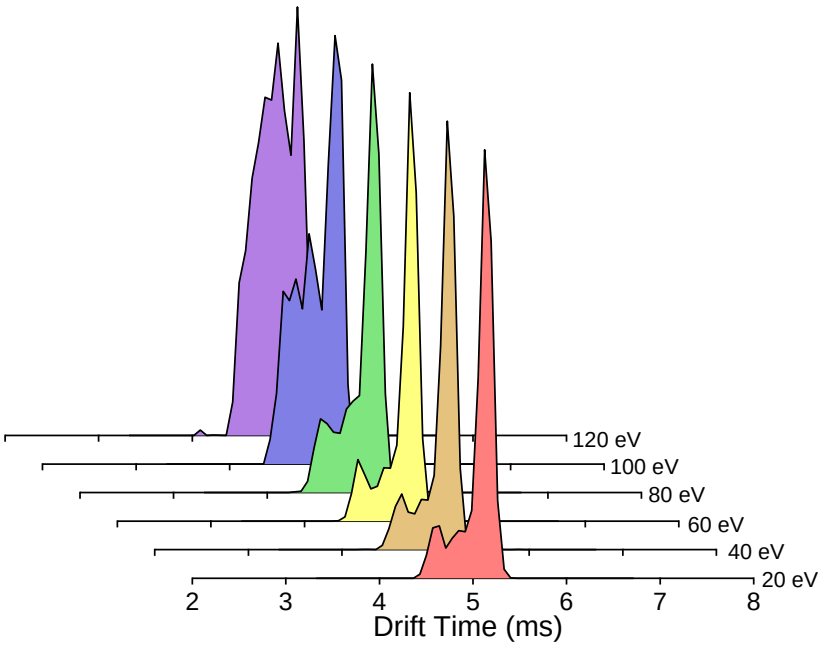

Figure S6: CID-IM drift time distributions of penetratin-Arg (5+) using 20-120 eV activation energy in the trap traveling wave ion guide of a Synapt G2 mass spectrometer. Dissociation occurs concomitantly with a reduction of the abundance of the more elongated population, suggesting it is the most labile. Note that all plots are normalized relative to the most abundant conformer, causing depletion of the extended conformation (the peak with the longer drift time). This makes it appear as though the more compact structures (peaks with shorter drift times) are becoming more abundant with increasing collision energy, when in actuality the abundances of the compact structures do no significantly change; rather it is the more extended conformation which diminishes.

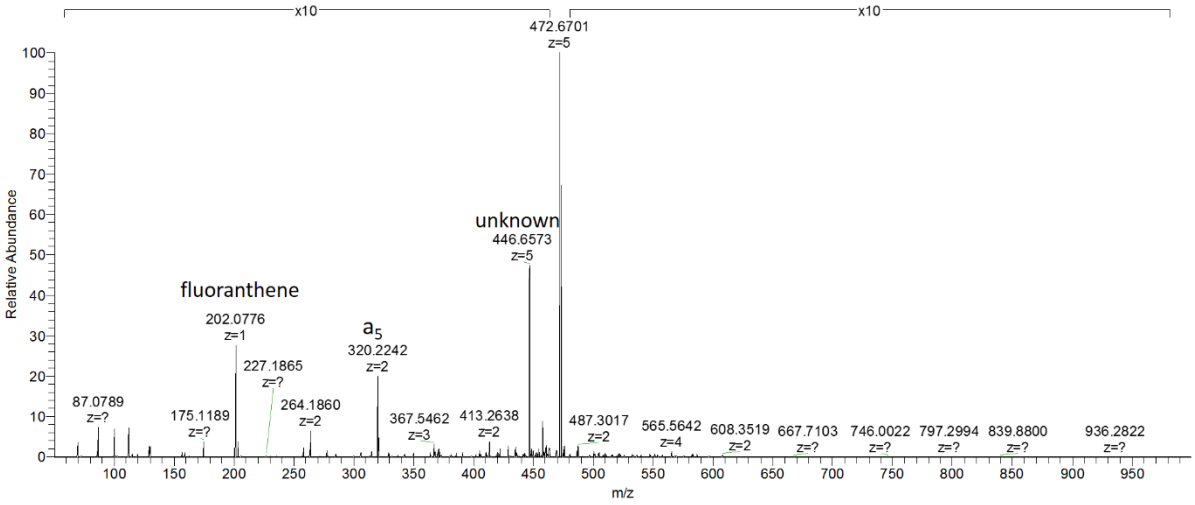

Figure S7: Mass spectrum of penetratin-Arg (5+) following UVPD (1 pulse , 1.5 mJ). The a_5 ion (2+) is significantly more abundant than all other *a/b/c/x/y/z* ion fragments, suggestion usual chemistry or overlapping fragments are confounding the determination of the α_a value for this cleavage site.

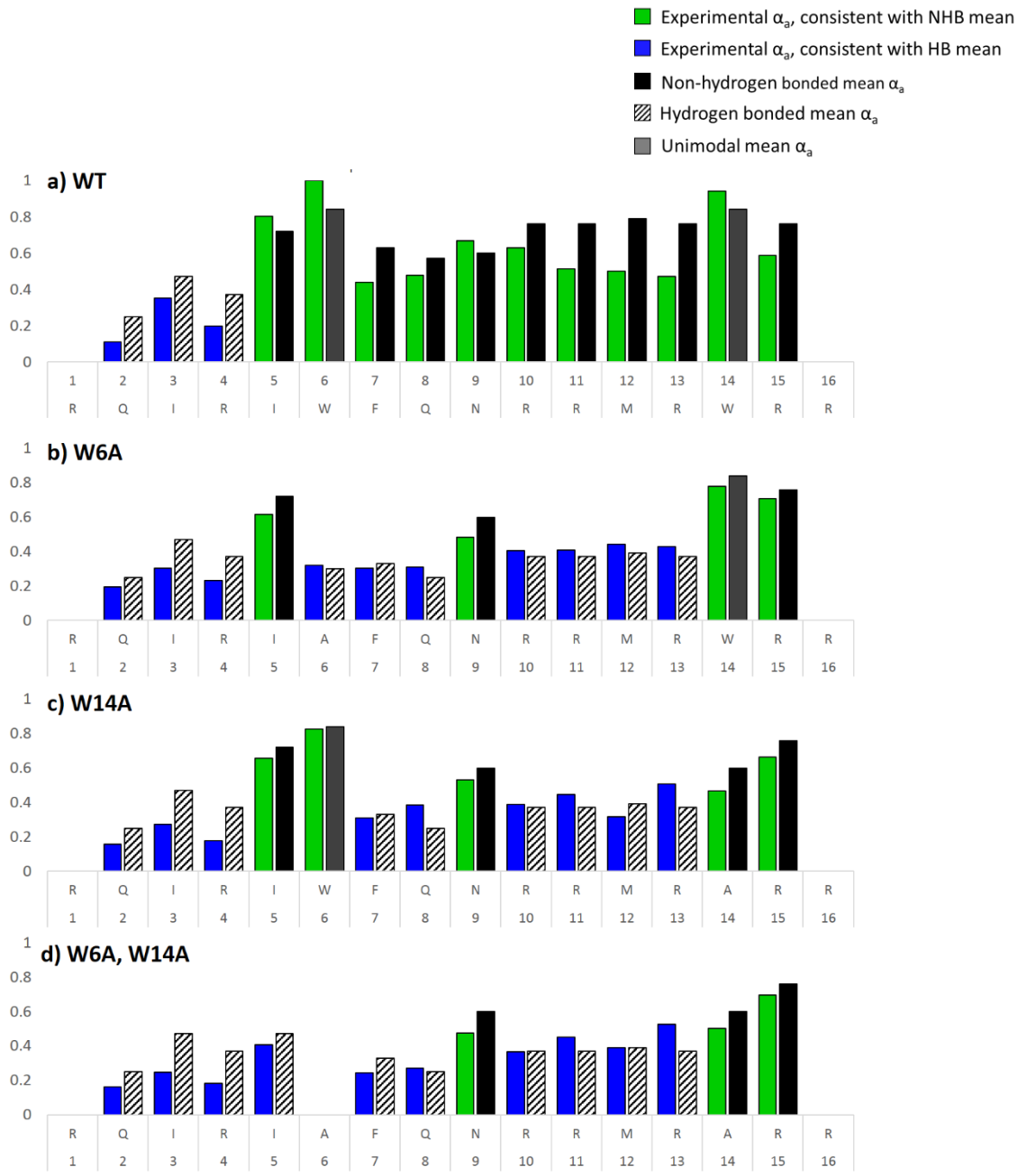

Figure S8. α_a values for penetratin-Arg variants in the 3+ charge state. (a) WT PA, (b) W6A, (c) W14A, and (d) W6A/W14A.

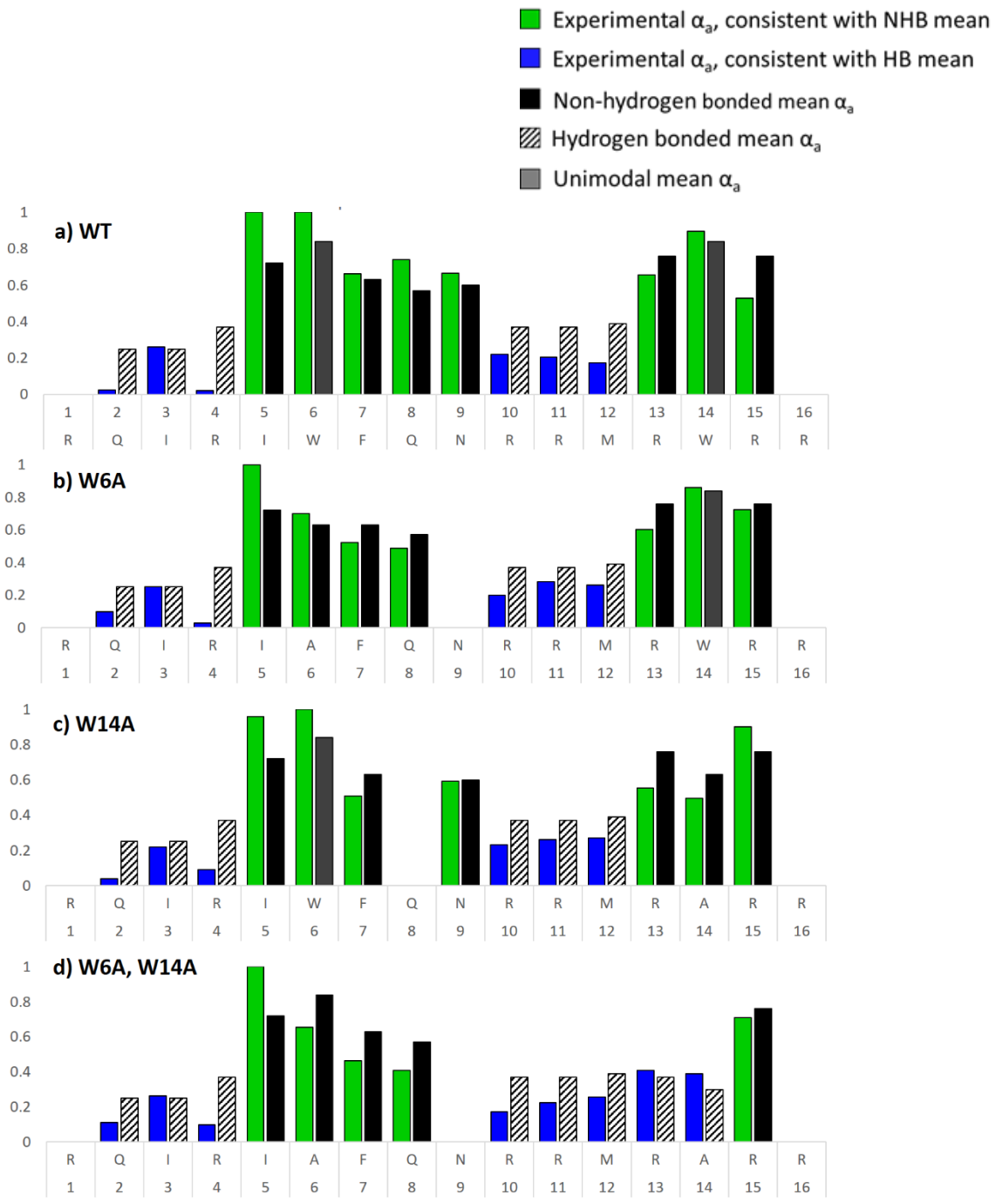

Figure S9. α_a values for penetratin-Arg variants in the 4+ charge state. (a) WT PA, (b) W6A, (c) W14A, and (d) W6A/W14A.

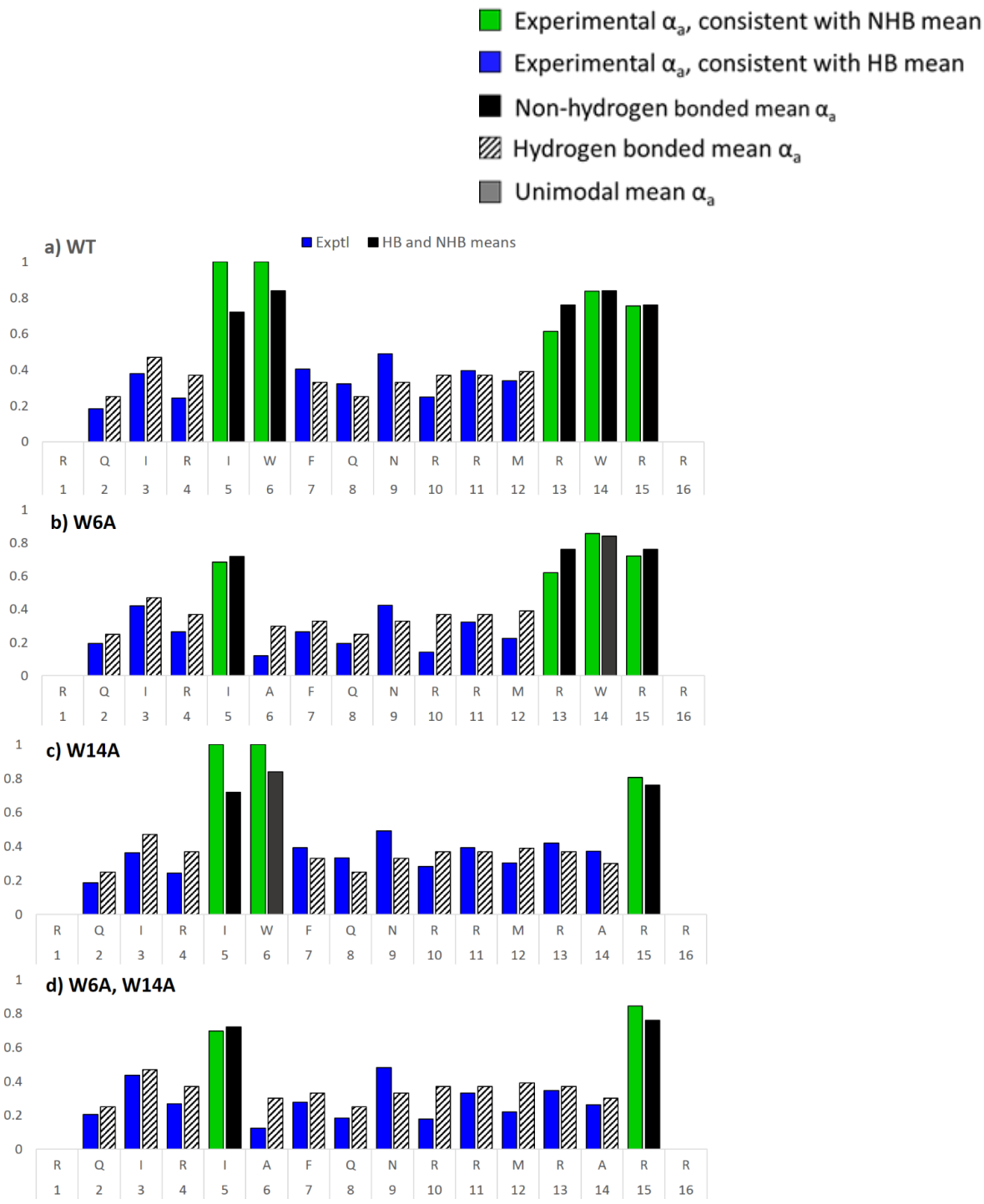

Figure S10. α_a values for penetratin-Arg variants in the 5+ charge state. (a) WT PA, (b) W6A, (c) W14A, and (d) W6A/W14A.

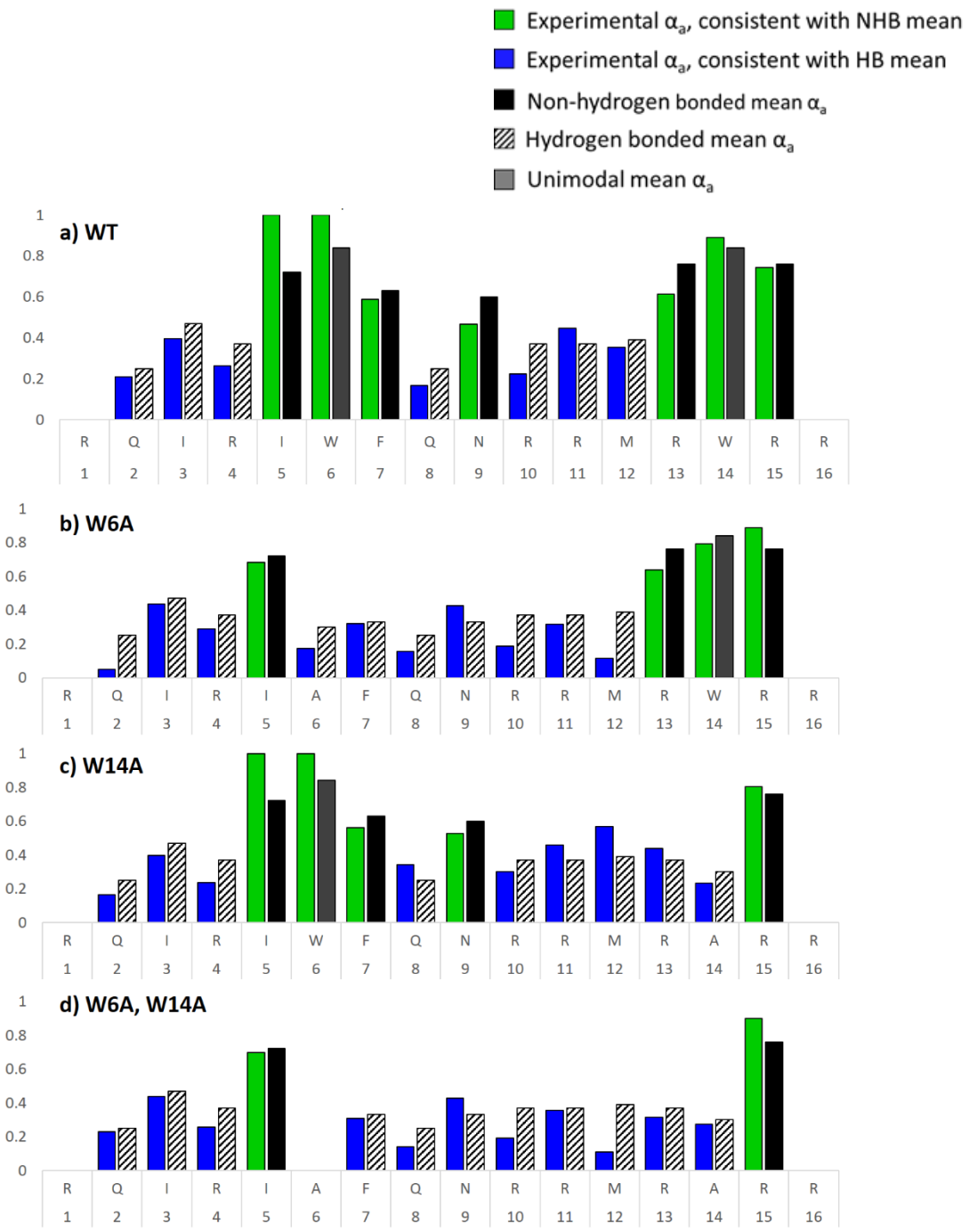

Figure S11. α_a values for penetratin-Arg variants in the 6+ charge state. (a) WT PA, (b) W6A, (c) W14A, and (d) W6A/W14A.

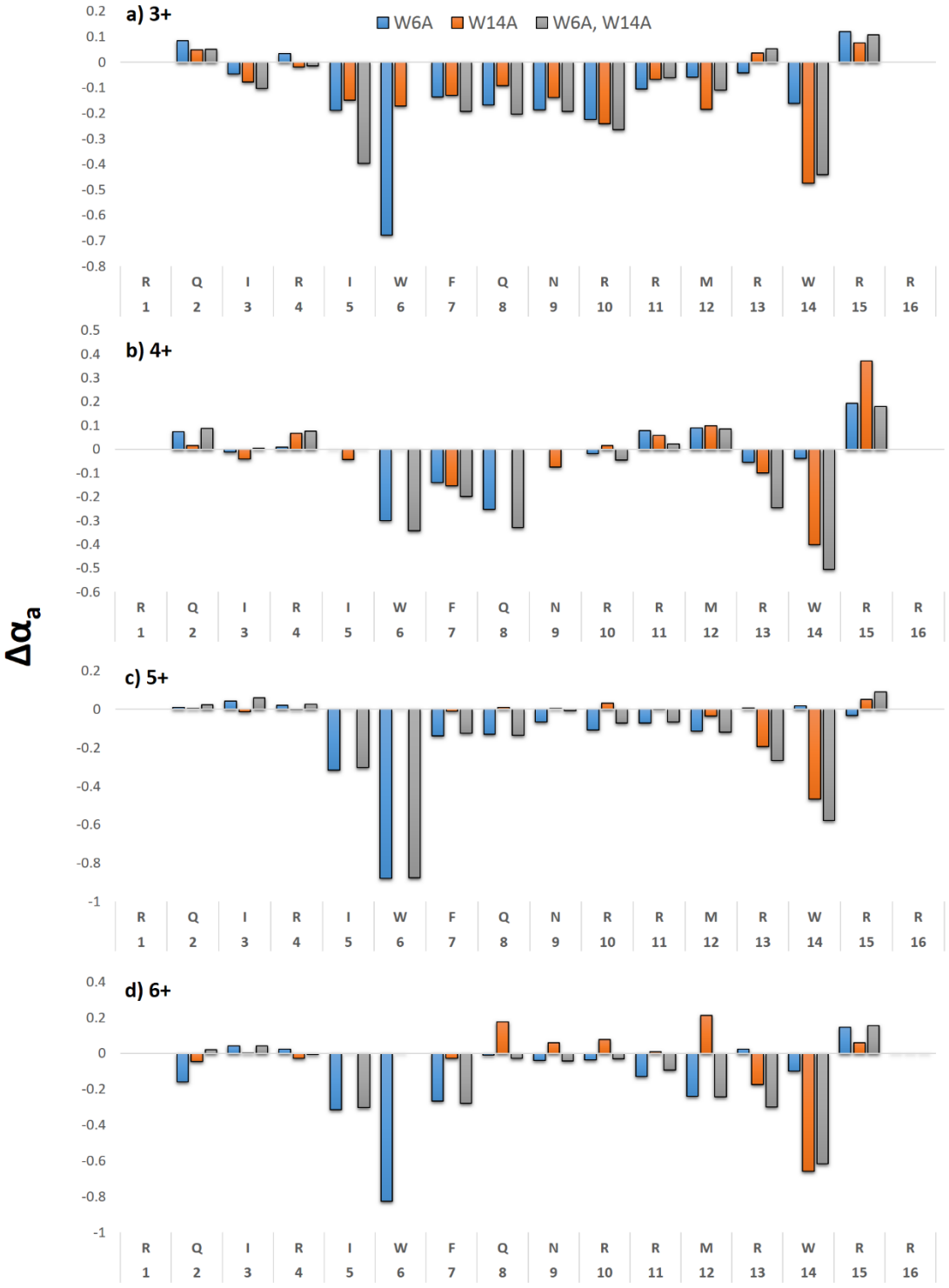

Figure S12: $\Delta\alpha_a$, defined as α_a[variant] – α_a[WT], is plotted for the (a) 3+ charge state, (b) the 4+ charge state, (c) the 5+ charge state, and (d) the 6+ charge state for three penetratin-Arg analogs (W6A (blue bars); W14A (orange bars); W6A,W14A (gray bars)) relative to penetratin-Arg.

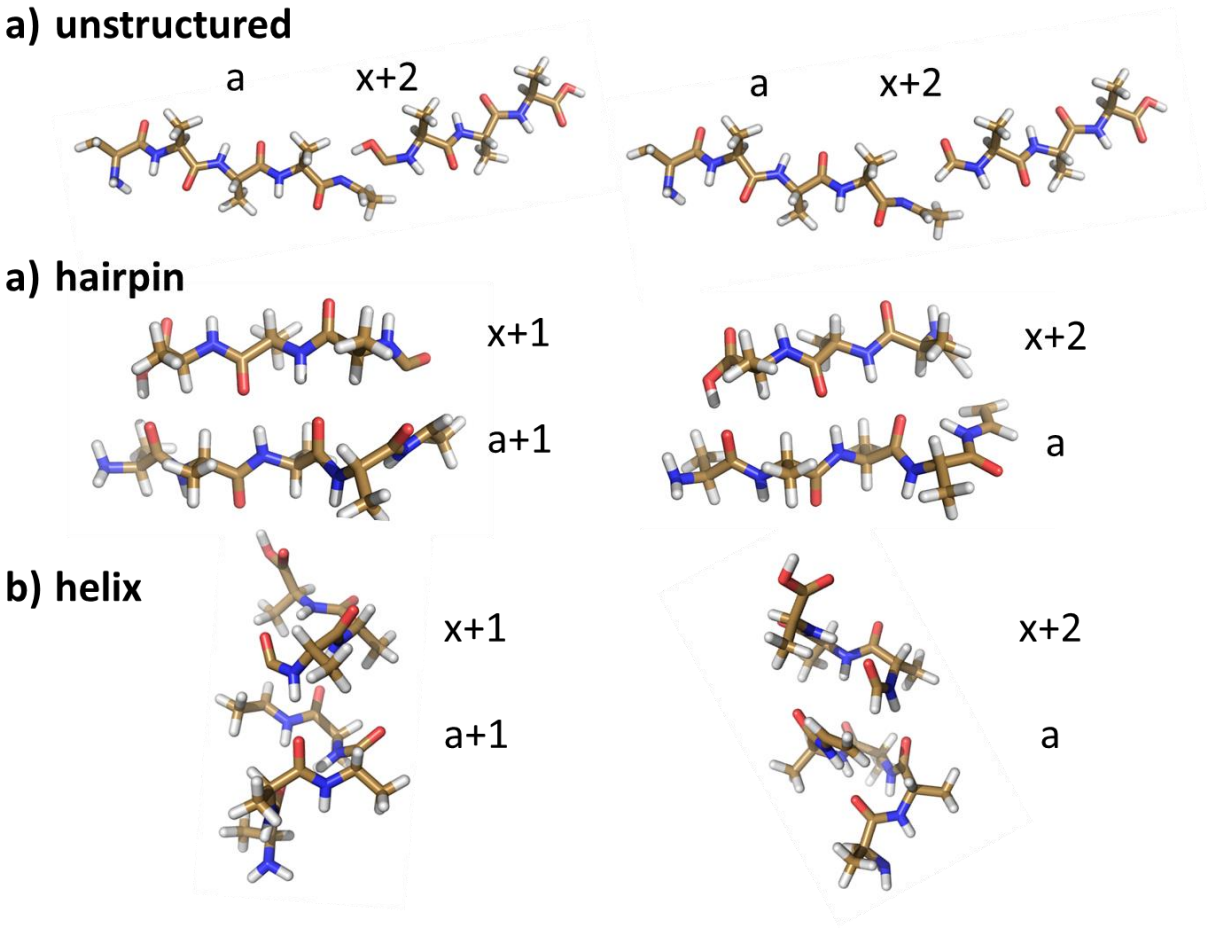

Figure S13: Full structures of fragment ions shown in Figure 4.

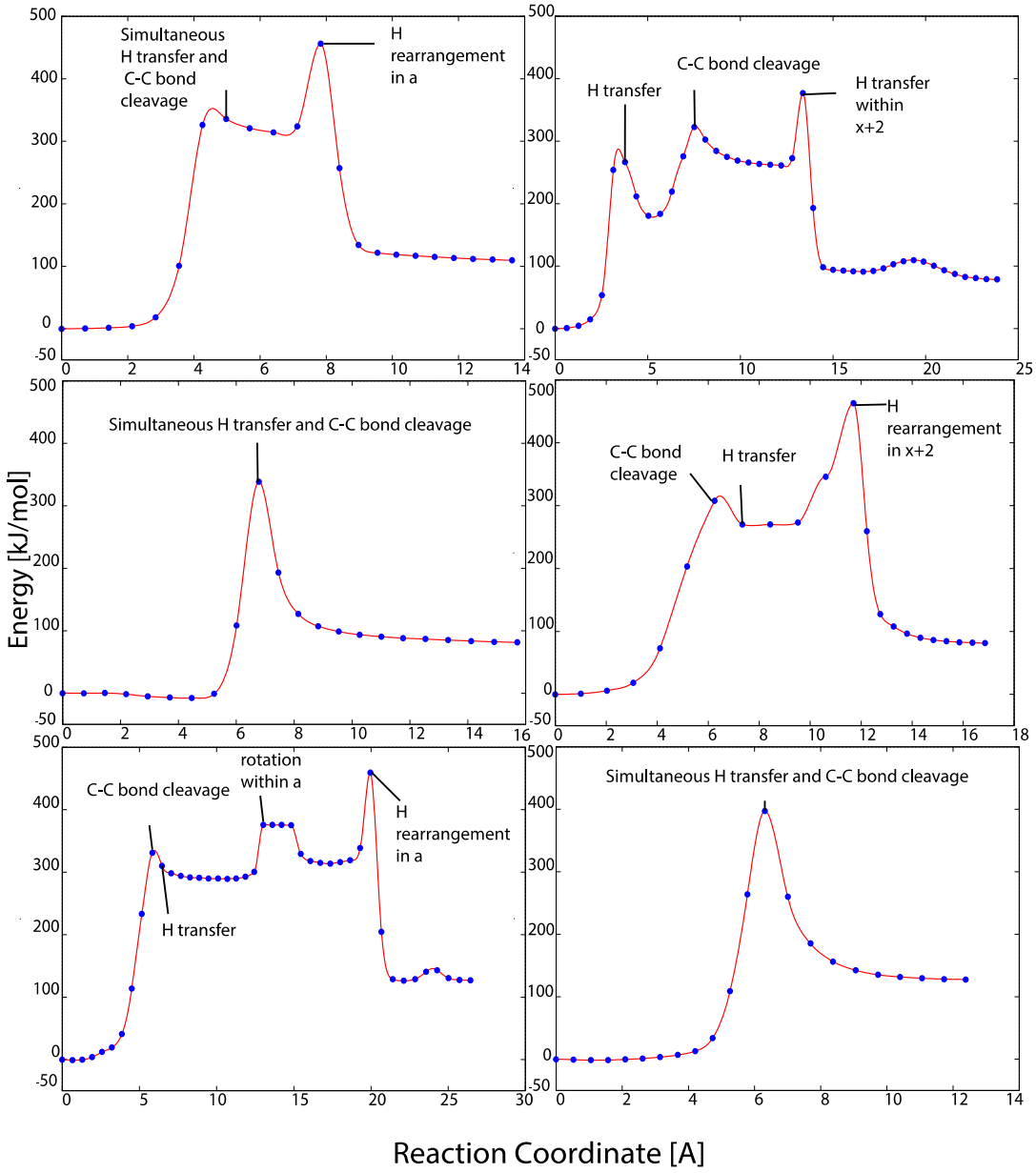

Figure S14. Additional MEPs for other pathways not shown in the main text. Panels correspond to: alpha hydrogen transfer (top left) and beta hydrogen transfer (top right) for an unstructured peptide; amide hydrogen transfer (middle left) and alpha hydrogen transfer (middle right) for a hairpin turn conformation; and alpha hydrogen transfer (bottom left) and amide hydrogen transfer (bottom right) for an alpha helix conformation. The reaction coordinate is the collective distance of atomic motion along the minimum energy pathway.

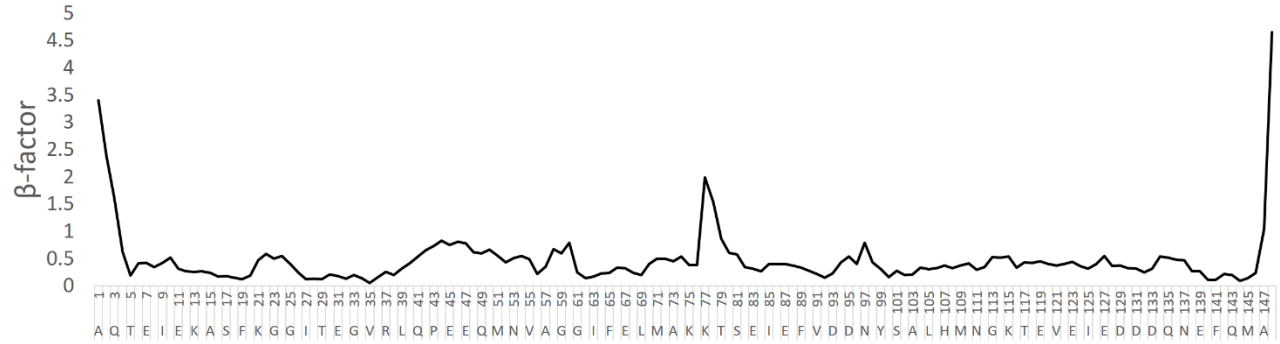

Figure S15: B-factors (from pdb 1CFC) versus sequence for apo calmodulin. B-factor is a crystallography packing parameter and correlates with protein flexibility and disorder.

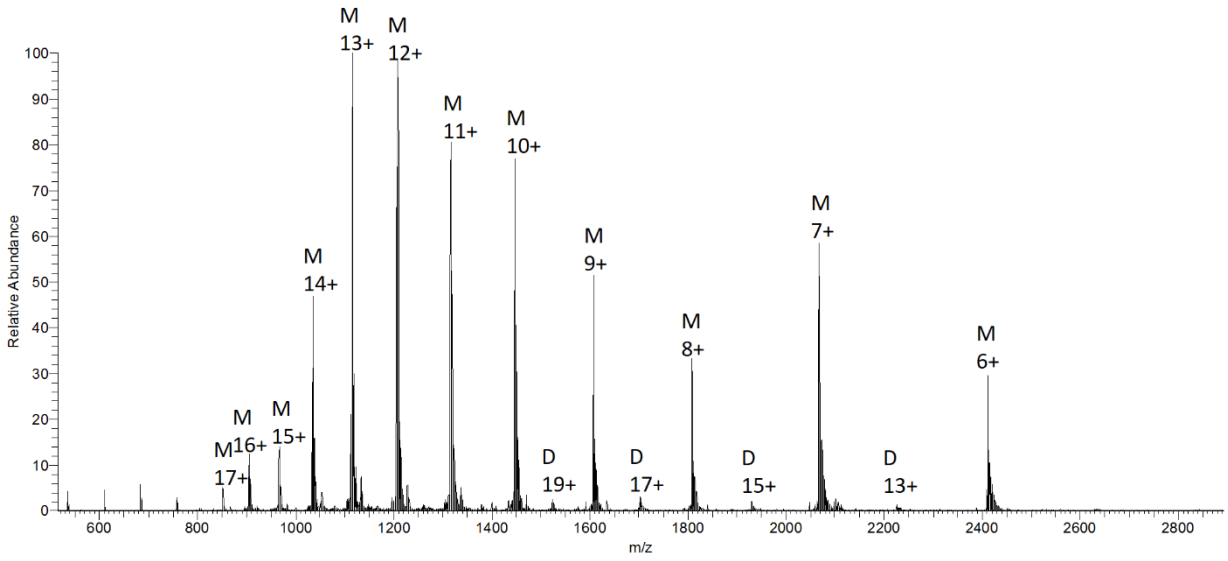

Figure S16: Mass spectrum of alpha-synuclein at pH 7. The letter “M” denotes monomer peaks and the letter “D” denotes dimer peaks.

	Amide H Transfer Pathway Dissociation Barrier (kJ/mol)	Alpha H Transfer Dissociation Barrier (kJ/mol)	Beta H Transfer Dissociation Barrier (kJ/mol)
Unstructured	288	352*	323*
Hairpin	339	315**	264**
Alpha Helix	397	335**	313**

Table S1. Energy barriers for hydrogen transfer. Barriers marked with * indicate that a hydrogen atom transfers before the C-C bond is broken; ** indicate that a hydrogen atom transfers after the C-C bond is broken. For all others, the hydrogen atom transfer and C-C bond breaking are concerted.